Disentanglement of electron dynamics and space-charge effects in time-resolved photoemission from *h*-BN/Ni(111)

Dominik Leuenberger,[*] Hirofumi Yanagisawa,[†] Silvan Roth, Jürg Osterwalder, and Matthias Hengsberger

Physik-Institut der Universität Zürich, Winterthurerstrasse 190, CH-8057 Zürich, Switzerland

We observe time-resolved and polarization dependent two-, three-, and four-photon transitions from a Ni(111) surface covered with a monolayer of hexagonal boron nitride. The spectra show features due to transitions involving two unoccupied intermediate states: the $n = 1$ image potential state of Ni(111) and a boron nitride-related interface state. We use these transitions in order to track the effects of space-charge on the spectra in view of pump-probe experiments, at high excitations densities. A simple model is presented, which reproduces the measured energy shifts and broadenings in great detail, allowing the ultrafast dynamics and the space-charge effects to be disentangled. Moreover, owing to the high excitation densities an additional particular three-photon transition via both the interface state and a virtual intermediate state could be measured and identified. The polarization-dependent transient of this transition has successfully been simulated, allowing the lifetime of the involved intermediate state to be extracted from the data.

I. INTRODUCTION

The transient structural, electronic, and magnetic responses of a condensed-matter system to the perturbation by intense femtosecond pulses have been successfully studied by time-resolved photoemission (tr-PE) in numerous experiments. Prominent recent examples are the transient melting of a charge density wave in TbTe$_3$,[1] the photo-induced vaporization of a charge-ordered state in 1T-TiSe$_2$,[2,3] and the ultrafast demagnetization in ferromagnetic thin films of nickel[4] or cobalt.[5] In all these studies, the system is excited by an intense (usually infrared) light pulse and the evolution of the spatial, electronic, or magnetic structure is subsequently probed by means of a second-, third-, or higher-harmonic pulse with photon energies between 3 eV and the extended uv range. Moreover, attosecond streaking experiments on solid surfaces[6] also deal with high fluences in the order of several mJ/cm^2.

At such high excitation densities, a high photoelectron background due to direct multiphoton absorption from the infrared pump pulse severely distorts the spectra in time-resolved experiments. On their drift to the detector after emission, all electrons interact strongly, exchanging kinetic energy due to mutual Coulomb repulsion. This leads to shifts and broadening of the spectral distribution, a phenomenon called space-charge effects. Previously, Siwick and coworkers studied quantitatively the effects of Coulomb repulsion in propagating charged clouds in electron guns.[7] The velocity and, thereby, temporal broadening of such electron pulses limits the time resolution in time-resolved electron microscopy or time-resolved electron diffraction experiments. More recently, Passlack *et al.* measured the $\sqrt{N}$ dependence (N denotes the number of simultaneously emitted electrons) of the spectral broadening of a Shockley surface state on Cu(111) with angle-resolved photoelectron spectroscopy.[8] Similar observations were made in experiments using undulator-based 3rd generation synchrotron radiation[9] or free-electron lasers,[10,11] where in particular high-brilliance free-electron laser sources provide photons in the extreme ultraviolet up to the soft x-ray regime with extremely high pulse densities and high photoelectron yields.

The goal of the present work is to disentangle space-charge effects from the underlying dynamics probed in multiphoton transitions from a model system on a femtosecond timescale. Two-color pump-probe experiments were carried out with intense infrared (800 nm, "red") pump pulses at a fluence of 3 mJ/cm^2 and frequency-doubled ("blue") probe pulses. The investigated system is a Ni(111) surface covered by a perfectly lattice-matched monolayer of hexagonal boron nitride *h*-BN. The unoccupied electronic structure of *h*-BN/Ni(111) has recently been studied in our group by means of time-resolved two-photon-photoemission (2PPE).[12] In this oscillator-based experiment at low pulse intensities and MHz repetition rate, possible space-charge effects were smaller than the energy resolution of the analyzer. Complementary information about the unoccupied band structure has been obtained by means of spin-resolved inverse photoemission (sr-IPE).[13] Two distinct intermediate states between the Fermi level and the vacuum level have been detected in 2PPE, both populated by excitation from the 3*d* bands of Ni(111). One of these intermediate states is the $n = 1$ image potential state (IPS) of the nickel substrate with a remarkably long lifetime of 261 fs; the other one is a *h*-BN-derived interlayer or interface state with a lifetime of 107 fs.[12]

First, we give an overview of the energetics (Sec. III) and dynamics (Sec. IV) of the system under investigation. Spectral distortions driven by mutual coulomb repulsions of the photoelectrons were observed at high excitation densities and a simple but complete space-charge model is introduced in Sec. V and applied to the time-resolved experimental data. Polarization-dependent probing of the dynamics (Sec. VI) reveals effects that go beyond this model and that can be explained in terms of lifetimes and symmetries of the two involved intermediate states.

II. EXPERIMENTAL SECTION

The light pulses were produced by means of a commercial femtosecond oscillator (Coherent Mira Seed) and amplified in a high repetition rate (250 kHz) regenerative pulse amplifier
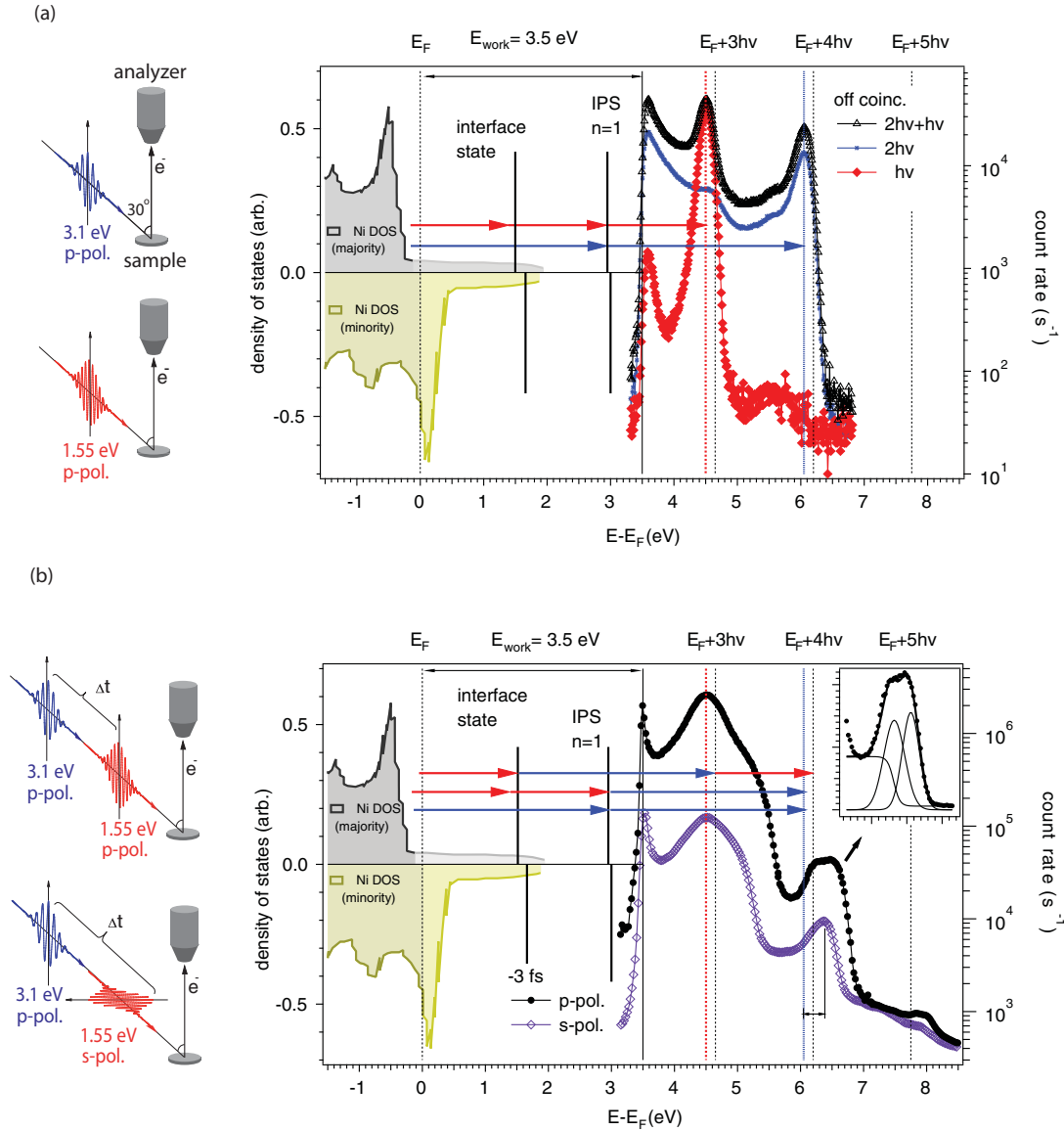
FIG. 1. (Color online) Spectra and direct transitions. Left-hand side: measurement geometry with the corresponding light polarization. Right-hand side: (a) Monochromatic photoelectron spectra at $\bar{\Gamma}$ for *p*-polarized fundamental light (1.55 eV; open diamonds), *p*-polarized SH light (3.1 eV; open circles), and a bichromatic spectrum using both wavelengths for large time delay (open triangles). (b) Bichromatic photoelectron spectra at zero delay between the *p*-polarized SH pulse and the intense fundamental pulse (open circles, *p*; open squares, *s*-polarized light). The initial states (occupied DOS of Ni) and the unoccupied intermediate states of the indicated multiphoton transitions are given. Inset: In the case of the *p*-polarized fundamental, the IPS signal exhibits two peaks (fitted by two Gaussians). The low-energy peak corresponds to an excitation via the IPS, the one at higher kinetic energy via the interface state.

(RegA 9050). On the sample, the fundamental (red, 800 nm, 1.55 eV) pulses were polarized with the electric field vector either in or perpendicular to the plane of incidence, referred to hereafter as *p*- or *s*-polarization, respectively, as schematically drawn in Fig. 1. Part of the fundamental light was frequency-doubled (blue, 400 nm, 3.1 eV) in a 0.5-mm-thick β-barium borate crystal; the group velocity dispersion was compensated in a prism sequence. The second harmonic (SH) light was *p*-polarized in order to excite electrons via the IPS or the interface state into a free electron final state in vacuum.[12] The pulse widths were 108 and 70 fs at the sample position for the fundamental and the SH, respectively. Since the blue-blue transition via the IPS is a

2PPE process, the effective probe pulse width is $70/\sqrt{2} \approx$ 50 fs, leading to an overall cross-correlation width of 119 fs.[14]

The red pulses were delayed on a computer-controlled delay stage. Both light beams were focused onto the sample inside an ultrahigh vacuum photoemission chamber[15] using a lens of 300-mm focal length, which produces a spot with a beam waist of about 100 μm. The pump fluence of the red pulses was set to 3 mJ/cm^2 on the sample, which corresponds to 140 nJ of absorbed pump energy ($5.6 \cdot 10^{11}$ photons) per pulse in the probed volume. The total number of photoelectrons per pulse has been determined by measuring the sample current with a pico amperemeter (Keithly 6487).

The photoemitted electrons were analyzed in a hemispherical VG ESCALAB 220 energy analyzer[15] with energy and angular resolution set to 50 meV and $\pm 1°$, respectively. All spectra shown were taken with a bias voltage of -10 V applied to the sample with respect to the analyzer in order to avoid the low-transmission regime of the analyzer at low kinetic energies.[16]

The h-BN monolayers were grown on a Ni(111) single crystal under ultrahigh vacuum conditions (base pressure of 10^{-10} mbar) by chemical vapor deposition of ~ 100 L (1 Langmuir $= 10^{-6}$ torr s) of borazine at a surface temperature of 1070 K.[17] The quality of the h-BN monolayer was verified by ultraviolet and x-ray photoelectron spectroscopy and low-energy electron diffraction.[18] Moreover, the work function of the sample was constantly monitored during the measurements by recording full 2PPE spectra. During all experiments, no irreversible change of the work function was observed: the h-BN monolayers remained stable under illumination with laser radiation and the chemical inertness allowed for long measurement periods under reproducible conditions.[19]

III. SPECTROSCOPY

The *monochromatic* 2PPE spectrum of h-BN/Ni(111) taken at normal emission with blue light exhibits two peaks [see Fig. 1(a)], which were previously investigated by Muntwiler *et al.*[12] The first one at 6.1 eV and the second one at 4.65 eV above E_F are both pumped from the initial states Λ_1 and Λ_3 lying in the bulk d-bands of nickel into the IPS and the interface state, respectively. Owing to the large band gap of more than 5 eV, the occupied σ and π valence bands of h-BN are out of reach of the experiment. The populated IPS is subsequently probed by absorption of a second photon as indicated by two horizontal arrows in Fig. 1(a).

The energy positions of the Rydberg series of the IPS on bare metal surfaces are pinned relative to the vacuum level and thus depend on the work function of the surface.[20,21] The presence of a dielectric layer on top of the surface leads to a net charge transfer from the boron nitride monolayer to the Ni substrate of 0.06 electrons per unit cell[22] and thus to a reduction of the surface dipole. As a consequence, the work function is only 3.6 eV as compared to 5.1 eV in the case of a bare Ni(111) surface. The metallic image potential is thereby modified in two ways[23]: first, an electron outside the surface polarizes the dielectric layer causing an attractive interaction, which tends to increase the binding energy E_B of the IPS. Second, the polarization of the dielectric layer screens electric fields between the metal and the electron resulting in a reduced IPS binding energy. In our case, screening by the boron nitride layer seems to dominate as a net reduction of the binding energy is found for h-BN/Ni(111) (600 meV with respect to the vacuum level[12]) as compared to pristine nickel (800 meV[24]).

The second peak at 4.65 eV above E_F corresponds to a h-BN-related unoccupied interface state theoretically predicted by density-functional theory (DFT).[22,25–27] According to the computations, this state is spatially located *between* the topmost Ni layer and the boron nitride layer. The ferromagnetic exchange splitting of the Ni $3d$ bands lifts the spin degeneracy of both the IPS and the interface state. sr-IPE locates the majority band bottom of the interface state at 1.7 eV above E_F

and gives a value of 150 meV for the exchange splitting,[13] in excellent agreement with DFT.[22] The absence of a photohole in the case of IPE might explain that the binding energy obtained from 2PPE data is lower by 190 meV than the results of IPE. Indeed, in a recent paper it was argued that perfect h-BN single crystals have exciton absorption bands with an exciton binding energy of 0.149 eV,[28] which gives evidence for the formation of an exciton out of the interface state in the 2PPE process.

A similar spectrum is obtained if only red light is used: here the low photon energy of 1.55 eV implies that only three- and four-photon processes contribute to the spectrum shown in Fig. 1(a). At 4.51 eV, a fairly strong feature shows up, which according to its energy position could involve both the IPS and the interface state. The bichromatic spectrum shown on top in Fig. 1(a), was taken using photons of both wavelengths, but for large time delays between both pulses in order to suppress all processes involving both wavelengths. As a consequence, the spectrum represents the sum of both monochromatic spectra.

IV. TIME-RESOLVED EXPERIMENTS

In Fig. 1(b), data are shown which were taken for both pump and probe pulses arriving at the same time on the sample, that is at zero delay. Three striking differences with respect to the data off coincidence, i.e., for large delay as in Fig. 1(a), can be observed: first, the intensity at 4.51 eV is greatly enhanced; second, a broad shoulder of extra intensity is piling up at its high energy side; the third observation is that the position of the IPS peak is shifted from 6.1 to 6.4 eV. Moreover, in the spectra taken with p-polarized pump light in Fig. 1(b), the peak splits into two components as shown in the inset of Fig. 1(b).

Regarding the dominant feature appearing at 4.51 eV, we note that the difference in energy between the IPS and the interface state is 1.42 eV, hence close to the fundamental photon energy of $h\nu = 1.55$ eV (see discussion above). This means that two possible excitation pathways lead from the very same initial state to the same final state, as already conjectured in Ref. 12: one channel corresponds to a $red - blue$ process via the interface state, the second passing through the IPS in a $blue - red$ sequence. Interference between both channels leads to a strong resonance observed in the data shown in Fig. 1(b). For the following, it is important to note that the overall yield strongly increases for p-polarized pump light when pump and probe pulses overlap temporally, the same being true but to less extent for s-polarized pump light.

In the following discussion of the time-resolved data, we will mainly focus on the feature around 6.1 eV. The spectra are plotted against energy and time delay for s- and p-polarized pump light in Figs. 2(a) and 2(b), respectively. Again, around zero delay the position of the peak shifts toward higher energy and recovers approximately 200 fs after the pump pulse. In the data taken for p-polarized pump light in Fig. 2(b), the intensity of the IPS apparently decreases for small negative delays giving rise to the double-peak structure already observed in Fig. 1(b). The two peaks are separated by 235 meV at delay zero. Anticipating the results of the simulations, the one at lower kinetic energy belongs to a $blue - blue$ transition via the IPS, whereas the one at higher energy to a $red - blue - red$ transition via the interface state, which appears at slightly
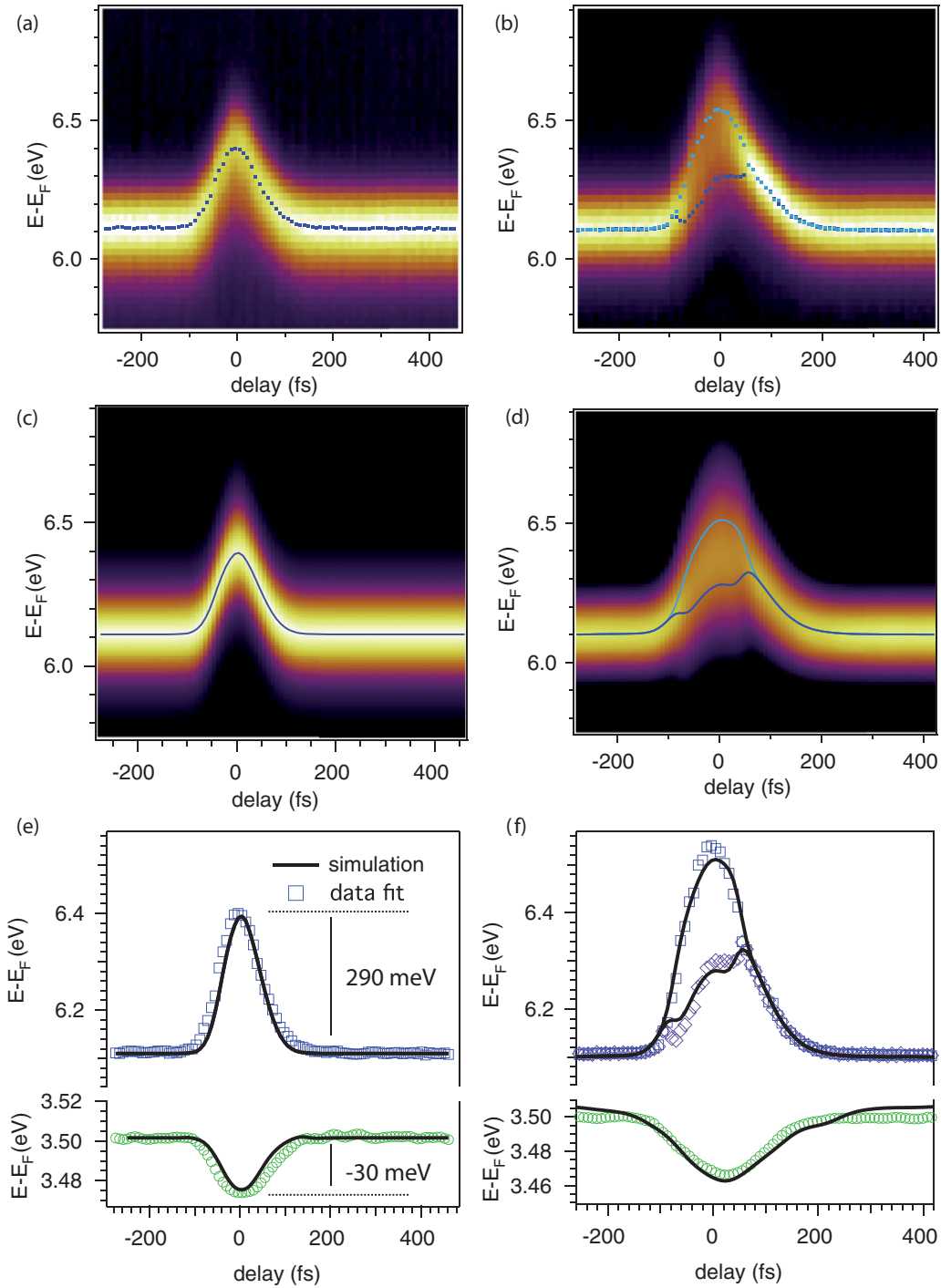
FIG. 2. (Color online) False-color plot of the photoemission intensity and corresponding simulations from the IPS as function of final state energy (vertical axis) and time delay with respect to *s*-polarized [data in (a), simulations in (c)] and *p*-polarized (b, d) fundamental pump pulses. The peak positions as found by fitting Gaussians are superimposed as solid symbols. In the bottom panels, the fitted energy positions of the peaks and of the secondary cut-off (open circles) are plotted as function of time delay for *s*-polarized (e) and *p*-polarized (f) pump pulses together with the results of the space-charge simulations (solid lines).

higher energy (see Fig. 3). Both peaks shift toward higher energy for small delays. While the hot-carrier dynamics associated with the high excitation density were the target of this study, the fact that many electrons (of the order of one thousand per pulse) are emitted simultaneously implies that the energy shifts are caused by Coulomb interactions during the drift of the photoelectrons to the detector. In order to recover

the underlying dynamics in the solid, a model was developed to account for such space-charge effects.

V. SPACE CHARGE DISK MODEL

For a quantitative analysis of the effects related to Coulomb repulsion during the drift to the detector, we recorded the
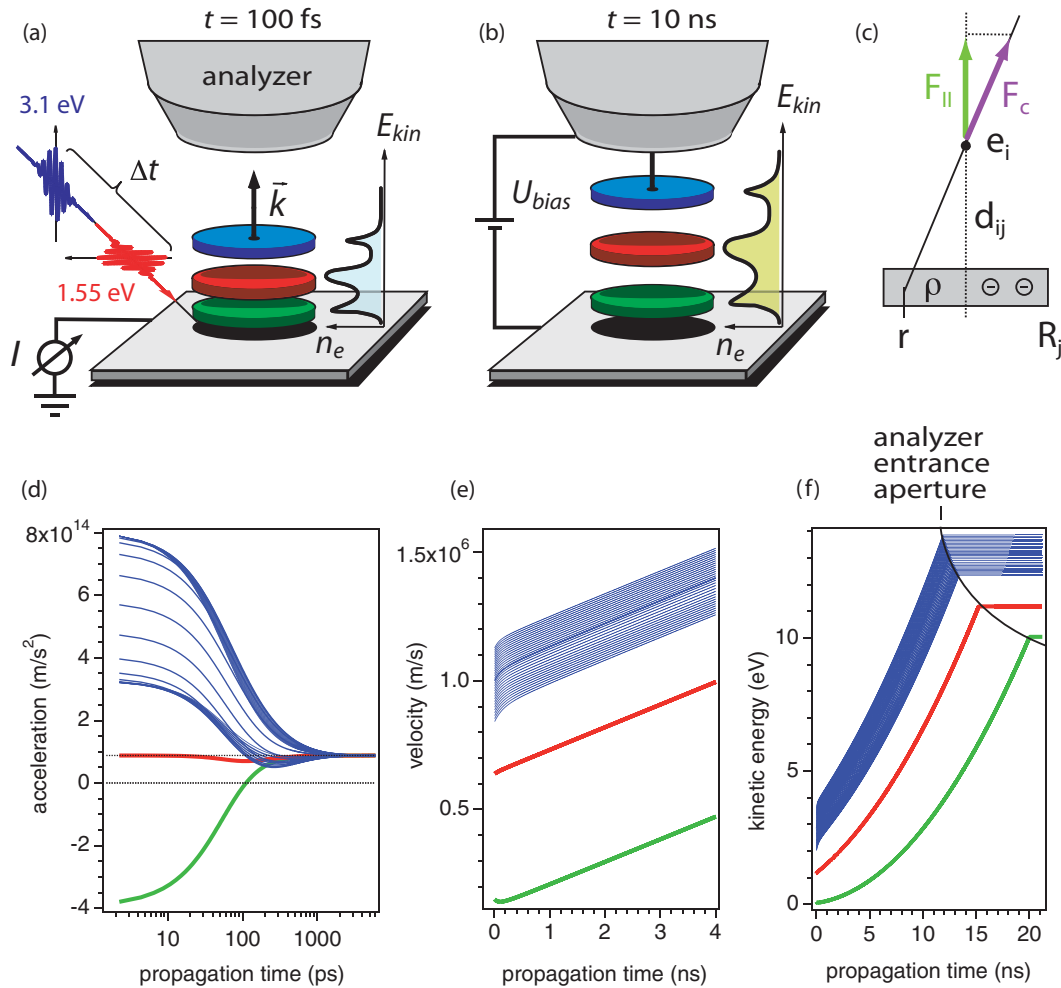
FIG. 3. (Color online) Simplified sketch of the space-charge model. The three dominant spectral features are represented by charged disks of photoemitted electrons corresponding to the IPS transition (top most disk, highest velocity), the resonant transition at $E_F + 3h\nu$ (center disk), and the inelastically scattered electrons from the secondary cut off (slowest disk) directly after emission (a) and after 10 ns drift (b). (c) Superposition of the repulsive coulomb forces among all the spectral features along the propagation direction to the analyzer leads to space-charge-induced broadening and energy shifts of the photoelectrons, exemplified here as the Coulomb force exerted by a space charge disk with radius R and charge density ρ onto a single electron e^- at a distance d. Calculated acceleration (d), velocity (e), and kinetic energy (f) of the IPS (upper trajectories), the resonance at 4.51 eV (central trajectory) and the secondary electrons (lowest trajectory) as function of propagation time toward the analyzer. For the IPS, all single trajectories are shown, for the other disks, only the motion of the center of gravity is plotted for the sake of clarity.

photoelectron spectra using blue pulses for delays in the range between -280 and 420 fs with respect to a s-polarized [Fig. 2(a)] and a p-polarized red pump pulse [Fig. 2(b)]. In the very first instance, when all electrons are released from the sample within roughly the duration of the probe pulse, each electron experiences some acceleration depending on the precise moment of emission. Since the latter is a result of a stochastic process, the energy distribution is only broadened. At later stages during drift, the spatial distribution of the electron cloud represents the velocity distribution, i.e., the spectrum. In a simplified picture the fastest electrons are pushed forward by the space charge cloud behind, while the slowest electrons are decelerated by the space charge in front. Therefore, the net acceleration depends on the longitudinal spatial position of the electrons and, thereby, on the velocity or else the kinetic energy of the electrons.

As a result, the kinetic energy of the IPS gradually shifts toward higher energies and the total energy shift depends on the absolute number of electrons emitted simultaneously. The total shift of the IPS reaches its maximum for delays at which the photoyield is the highest, i.e., close to zero delay: $\Delta E_{\rm kin} = E_{\rm kin}(0\,{\rm fs}) - E_{\rm kin}(-300\,{\rm fs}) = 290$ meV, as plotted in Fig. 2(e). At the same time, the maximum of the inelastically scattered secondary electrons is shifted in the opposite direction ($\Delta E_{\rm kin} = -30$ meV) upon going from negative delays to 0 fs and fully recovers for positive delays $\Delta t > 300$ fs.

To model these space-charge effects for each delay step Δt, we sliced the photoelectron spectrum into a series of 2D disks[7,8] with the thickness given by the kinetic energy spread in each disk and with the radius $R = 50\,\mu$m, corresponding to the laser beam waist on the sample taking into account second order nonlinearity of the 2PPE process.[8] The cartoon
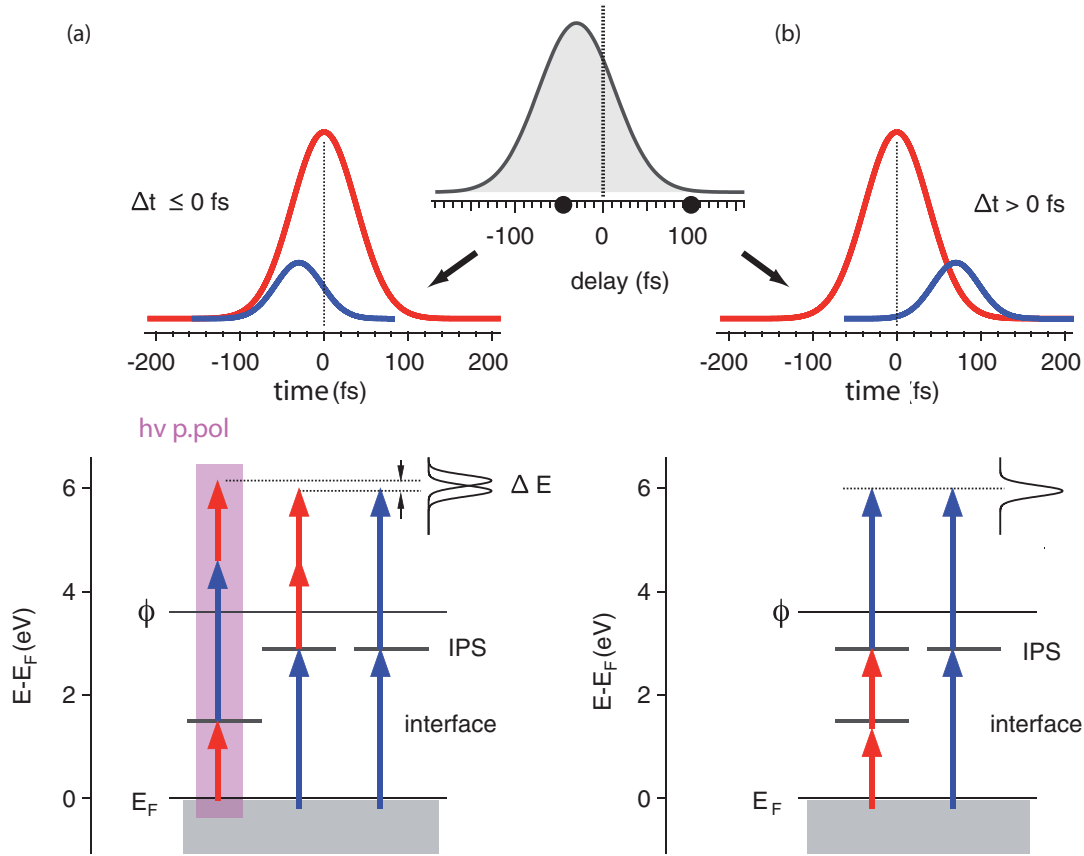
FIG. 4. (Color online) Possible 2PPE and 3PPE transitions with final free photoelectron energies around 6 eV for *p*-polarized fundamental (1.55 eV) and SH (3.1 eV) for small negative (a) and positive (b) time delays between fundamental and SH pulses. The gray shaded curve depicts the transition probability [Eq. (3)] for a *red-blue-red* 3PPE transition involving the interface state like shown by the arrows of the left most transition.

in Figs. 4(a) and 4(b) depicts three of them, the fastest disk for the IPS, the central one for the resonance at 4.51 eV, and the slowest disk for the secondary electrons. In the simulation i.e., the IPS was sliced into 91 disks corresponding to energy steps of 18 meV between two neighboring disks.

The total charge and the charge density $\rho(\Delta t)$ of each disk was computed from the measured total sample current I_{sample} and from the measured photoelectron spectrum $A(E, \Delta t)$ for each delay step Δt. Starting point for each delay Δt were energy positions of the three peaks according to a spectral distribution measured off coincidence ($\Delta t < -200$ fs) and, hence, at a nondistorted low-fluence condition. The relative intensity of the three spectral features for the simulation, namely, the IPS, the resonance, and the secondary cut off at a certain delay Δt, have then been obtained from the photoelectron intensities $A(E, \Delta t)$. For each of the three spectral features, integration over the distinct spectral range leads then to the delay dependent spectral weight $\omega(\Delta t)$ of the particular feature, i.e., for the IPS:

$$\omega(\Delta t)_{IPS} = \frac{\left[\int_{5.8eV}^{7.2eV} A(E, \Delta t) dE \right]}{\left[\int_0^\infty A(E, \Delta t) dE \right]}.$$

Finally, the total number of photoelectrons per delay step Δt given by the measured sample current $I_{sample}(\Delta t)$ has been

distributed among all the slices in the weighted spectrum. As an example, a current of 78 pA at zero delay and 250 kHz repetition rate corresponds to $N = 1950$ photoelectrons per pulse.

The initial angular distribution of the photoelectrons, defined by the opening angle of the emission cone θ_e and the electron trajectories under the influence of the applied bias field,[16] then determine the temporal evolution of the radius $R(t)$ and thus of the charge density $\rho(t)$ on the way to the detector.[29] In a first approximation, we neglect the lateral Coulomb repulsion and assume the charge density to be homogeneous over the whole 2D area.[7]

Finally, the Coulomb force $F_{c\parallel}^{ij}$ along the propagation direction exerted by the charge in disk j with radius R_j and comprising a fraction n_j of the total photoelectron yield onto a test electron e_i at a distance d_{ij} [see Fig. 4(c)] is then given by

$$F_{c\parallel}^{ij}(t) = \frac{n_j e^2}{4\pi \varepsilon_0} \cdot \int_0^{R_j(t)} \int_0^{2\pi} \frac{d_{ij}(t) \cdot r}{\left(r^2 + d_{ij}^2(t)\right)^{3/2}} \cdot dr \, d\varphi$$

$$= \frac{n_j e^2}{2\pi R_j^2(t) \varepsilon_0} \cdot \left[1 - \frac{d_{ij}(t)}{\sqrt{R_j^2(t) + d_{ij}^2(t)}} \right] \quad (1)$$

In the next time step of the numerical integration, each disk of photoelectrons i is then accelerated by the superposition of all mutual coulomb forces of all disks $j \neq i$ and by the

externally applied bias field between sample surface and analyzer entrance aperture ($U_{\mathrm{bias}} = -10$ eV over a distance D of 0.02 m):

$$m_e\, a_i(t) \;=\; \frac{e \cdot U_{\mathrm{bias}}}{D} + \sum_j F_{c\parallel}^{ij}(t). \qquad (2)$$

The initial kinetic energy E_{kin}^{i} of the photoelectrons just outside the surface was directly taken from spectra taken at low fluence: typically, values of 2.73 and 1.11 eV were used for the IPS and the resonance, respectively. The mean energy of the secondary electrons was set to 65 meV. Effects of the attractive image potential on the propagating spectral distribution have been discussed in previous publications[9,10,30] but were neglected in the present work. Acceleration $a(t)$, velocity $v(t)$, position $x(t)$, and kinetic energy $E_{\mathrm{kin}}(t)$ were iteratively calculated using Eqs. (1) and (2) for each time step of 2 ps for the drift between sample surface and detector entrance as shown in Figs. 4(d) through 4(f). The results of the simulations for time delays between -280 fs and 420 fs are shown in Fig. 2(c). The calculated shift in kinetic energy $\Delta E_{\mathrm{kin}} = 290$ meV and the additional broadening of the IPS by 28 meV between negative and zero delay are in excellent agreement with the experimentally obtained values of 280 and 30 meV, respectively. The more complicated case of the p-polarized pump pulse in Figs. 2(b), 2(d), and 2(f) will be discussed in Sec. VI.

Throughout the simulation, only the opening angle of the emission cone was *a priori* not known, because solely one angle should be used for the whole electron distribution in order to keep the calculations as simple as possible. The simulation was carried out for various values and the values were compared to results of angle-resolved 2PPE data afterwards. We obtained emission cones with opening angles of $6°$ and $10°$ for p- and s-polarized pump light, in very good agreement with previous experimental results.[12]

As expected from the calculated accelerations in Fig. 4(d), most of the energy exchange by means of Coulomb repulsion occurs within 1 ns after emission (in agreement with Refs. 3, 7, and 8). The bunch of decreasing trajectories in Fig. 4(d) represents the energetically sliced IPS into charged sub disks. Intrinsic broadening of the IPS is caused by slightly different slopes within the bunch. All curves shown in Fig. 4(d) converge asymptotically toward the same value, which is given by the external bias field applied between sample and analyzer entrance aperture. Eventually, it takes then 12 ns for the fastest and roughly 20 ns for the slowest electrons to reach the detector aperture, denoted by bended line perpendicular to the traces in Fig. 4(f).

VI. DYNAMICS BEYOND THE SPACE-CHARGE EFFECTS

The good agreement between the results of the space-charge model and the experimentally observed energy shifts suggests that the space-charge model catches the main physics in the time range within the pulse overlap, when the total yield strongly rises. The observed splitting of the IPS transition for negative delays and p-polarized fundamental infrared light [c.f. Figs. 1(b) and 2(b)] cannot be explained, however, by space-charge alone.

In order to get more insight, the spectral distribution between 5.9 and 6.6 eV above E_F was fitted by two Gaussians in the delay range between -80 and 60 fs [see the two distinct lines in Fig. 2(f)]. The fact that it essentially appears at negative delays means that the blue photons have to arrive before the red photons for the transition to happen. The only possibility beside the *blue-blue* and the *blue-red-red* transitions, both via the IPS with the same final energy, is given by a *red-blue* transition via the interface state followed by the absorption of another *red* photon in order to be excited to its final energy. Because of the high pump intensity, red photons are abundant as soon as the red pulse turns on. Hence, the peak measured at higher kinetic energy belongs to a *red-blue-red* transition first pumped by $h\nu$ into the interface state and subsequently probed by simultaneous adsorption of a $2h\nu$ and a $h\nu$ photon [sketched in Fig. 3(a)]. The 3PPE transition probability for this process as function of time delay Δt between $h\nu$ and $2h\nu$ is denoted as $P_{h\nu-2h\nu-h\nu}(\Delta t)$. It depends on the lifetime of the interface state ($\tau = 107$ fs) and the temporal widths of the two pulses.

Assuming the second peak component to be the result of the additional 3PPE transition, we can write the transition probability by means of the intensity correlation function of the pulses as follows:

$$S_0(\Delta t, t_0) \;=\; \int_{t_0}^{\infty} I_{2h\nu}(t - \Delta t)\, e^{-\frac{t-t_0}{\tau}}\, I_{h\nu}(t)\, dt,$$

where $\tau = 107$ fs denotes the lifetime of the intermediate interface state, and, finally,

$$P_{h\nu-2h\nu-h\nu}(\Delta t) \;\propto\; \int_{-\infty}^{\infty} I_{h\nu}(t_0)\, S_0(\Delta t, t_0)\, dt_0. \qquad (3)$$

$I_{h\nu}$ and $I_{2h\nu}$ are assumed to be Gaussians with full widths at half maximum (FWHM) of 108 and 70 fs for $h\nu$ and $2h\nu$, respectively (compare Sec. II). Equation (3) then yields an approximately Gaussian form for $P_{h\nu-2h\nu-h\nu}$ with the peak maximum at -30 fs and an FWHM of 67 fs (grey shaded areas in Fig. 3). We apply now the space-charge model for $N = 2400$ photoelectrons per pulse at zero delay corresponding to a sample current of 96 pA using the measured spectral distributions as function of delay time Δt and the calculated transition probability $P_{h\nu-2h\nu-h\nu}(\Delta t)$ from Eq. (3) for the 3PPE process. In contrast to the simulation with s-polarized red light, we add now in the case of a p-polarized red pulse a second peak 130 meV above the *blue-blue* transition (via IPS) corresponding to the *red-blue-red* transition (via interface state), weighted in intensity by the distribution $P_{h\nu-2h\nu-h\nu}(\Delta t)$. For an average emission cone of $\pm 6°$ opening, the calculation well reproduces the measured data as can be seen from comparing Figs. 2(b) and 2(d). Without space-charge effects, the final kinetic energy of the *blue-blue* transition and the *red-blue-red* transition would be separated by 130 meV. Mutual Coulomb repulsion between the emitted photoelectrons with slightly different kinetic energy and the slightly different acceleration caused by the other electrons at lower kinetic energy leads to a maximum difference ΔE_{kin} of 235 eV in the experimental data and 230 meV in the simulations for 0 fs time delay. Figure 2(f) shows the calculated and measured peak positions of these two features superimposed over the full time scale.
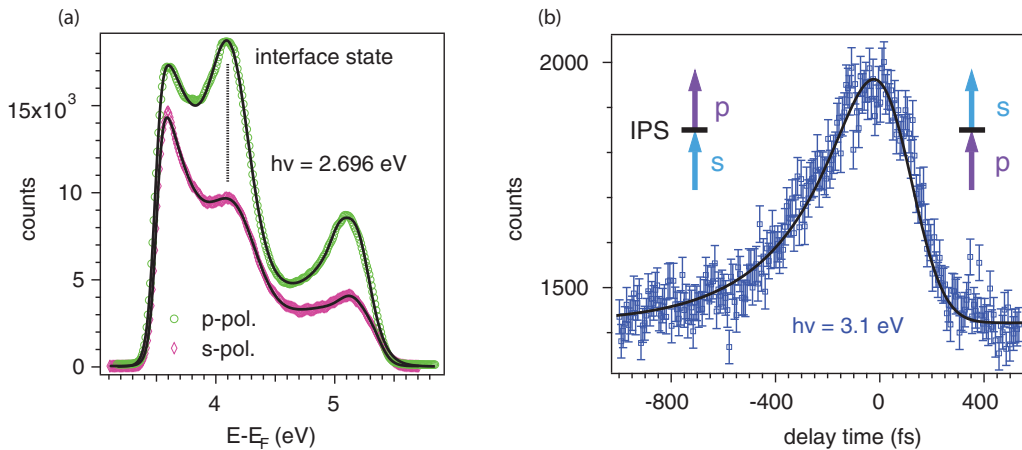
FIG. 5. (Color online) Time-resolved spectroscopy from interface and image potential states. (a) Monochromatic 2PPE spectra taken with either linearly *p*-polarized (open circles) or *s*-polarized (open squares) pulses with $h\nu = 2.696$ eV. The interface state as intermediate state and initial Ni *d* states are observed at 4.1 and at 5.1 eV above E_F, respectively. (b) Cross-correlation curve of the $n = 1$ image potential state as function of delay between the *s*- and *p*-polarized SH pulses. The photon sequence is indicated; the solid line is the solution of the rate equation for a lifetime of $\tau = 265$ fs.

Further evidence for the assumption of a 3PPE process via the interface state comes from polarization-dependent measurements. This transition only occurs in the case of a *p*-polarized red pulse. The measured photoemission intensity is proportional to the square of the matrix element

$$T_{fm} = \langle \psi_f | A \cdot \nabla | \psi_m \rangle,$$

where ψ_m is the intermediate interface state and ψ_f denotes a free-electron final state. Pure hexagonal BN has D_{6h} symmetry.[26] The corresponding interface state belongs to the Γ_1^+ representation in the notation of Robertson[31] and is even under reflection σ_h at the mirror planes.[25] Thus, T_{fm} is finite only for *p*-polarized light.[25,32] Indeed, monochromatic 2PPE measurements with 2.7 eV photon energy show a strong polarization dependence of both the intermediate interface state and the initial Ni 3*d* bands as can be seen in Fig. 5(a).

The same approach can be used to disentangle pump and probe pulses in monochromatic 2PPE experiments: the IPS, which has the same parity under reflection at the mirror planes as the interface state, can only be probed using *p*-polarized light. The pump, however, can be of either polarization, as initial states of different symmetry are available leading to finite momentum matrix elements also for *s*-polarized excitation.[33] Data for a two-photon sequence of same photon energy but different polarization are shown in Fig. 5(b): here, negative delays correspond to *s*-polarized pump and *p*-polarized probe and positive delays to the opposite sequence. The transient photoemission intensity is asymmetric with respect to zero delay showing an exponential decay with a time constant of 265 fs toward negative delays. We conclude that the IPS can only be observed using *p*-polarized excitation light in accordance with our analysis of the interface state above. The time constant is in excellent agreement with the IPS lifetime found in previous experiments.[12] It is noted in passing that as a consequence, the 4PPE transition observed at around 8 eV [*red-blue-red-red* in Fig. 1(b)] can only be detected in the case of a *p*-polarized fundamental pulse.

VII. CONCLUSIONS

Hexagonal boron nitride on Ni(111) represents an excellent model system for two-photon photoemission as it provides two well-separated unoccupied states of different character with high transition matrix elements for low-energy photons of suitable polarization.

In this work, we present data taken with multiphoton photoemission under high-excitation density. Three- and four-photon processes can be observed at high fluences of typically $>10^{13}$ photons per pulse or 3 mJ/cm^2. These transitions can be switched on and off by choosing either linearly *p*- or *s*-polarized red pulses, respectively, owing to the even parity of the intermediate state wave function under reflection at the mirror planes of the surface. The measured probability amplitude of a particular three-photon transition can be calculated using the known lifetime of the involved intermediate states and the cross correlation width of the femtosecond laser pulses.

Due to the large number of photoelectrons per pulse space-charge-related energy shifts of up to about 300 meV occur in the measured spectra. These space-charge-distorted spectra can be fully reproduced by simulating the propagation of a charged-disk ensemble representing the energy distribution of the photoelectrons in a simple model as function of pump-probe delay. All input parameters for these calculations can easily be obtained from the experiment itself, allowing the underlying electron dynamics inside the solid to be disentangled from the space-charge effects. We anticipate that this kind of data treatment will be essential for future studies using high-intensity streaking fields in attosecond experiments[6] or at free-electron laser sources.[10]

*leuenber@physik.uzh.ch

†Present address: Institut für Quantenelektronik, ETH Zürich, CH-8093 Zürich, Switzerland.

[1] F. Schmitt *et al.*, Science **321**, 1649 (2008).

[2] T. Rohwer *et al.*, Nature (London) **471**, 490 (2011).

[3] S. Hellmann *et al.*, Phys. Rev. Lett. **105**, 187401 (2010).

[4] H.-S. Rhie, H. A. Dürr, and W. Eberhardt, Phys. Rev. Lett. **90**, 247201 (2003).

[5] M. Cinchetti, M. Sánchez Albaneda, D. Hoffmann, T. Roth, J.-P. Wüstenberg, M. Krauß, O. Andreyev, H. C. Schneider, M. Bauer, and M. Aeschlimann, Phys. Rev. Lett. **97**, 177201 (2006).

[6] A. L. Cavalieri *et al.*, Nature (London) **449**, 1029 (2007).

[7] B. J. Siwick, J. R. Dwyer, R. E. Jordan, and R. J. D. Miller, J. Appl. Phys. **92**, 1643 (2002).

[8] S. Passlack, S. Mathias, O. Andreyev, D. Mittnacht, M. Aeschlimann, and M. Bauer, J. Appl. Phys. **100**, 024912 (2006).

[9] X. J. Zhou, B. Wannberg, W. L. Yang, V. Brouet, Z. Sun, J. F. Douglas, D. Dessau, Z. Hussain, and Z.-X. Shen, J. Electron Spectrosc. Relat. Phenom. **142**, 27 (2005).

[10] A. Pietzsch *et al.*, New J. Phys. **10**, 033004 (2008).

[11] K. Moribayashi, Phys. Rev. A **80**, 025403 (2009).

[12] M. Muntwiler, M. Hengsberger, A. Dolocan, H. Neff, T. Greber, and J. Osterwalder, Phys. Rev. B **75**, 075407 (2007).

[13] K. Zumbrägel, K. Wulff, C. Eibl, M. Donath, and M. Hengsberger, Phys. Rev. B **78**, 085422 (2008).

[14] S. Roth, D. Leuenberger, J. Osterwalder, J. E. Dahl, R. M. K. Carlson, B. A. Tkachenko, A. A. Fokin, P. R. Schreiner, and M. Hengsberger, Chem. Phys. Lett. **495**, 102 (2010).

[15] T. Greber, O. Raetzo, T. J. Kreutz, P. Schwaller, W. Deichmann, E. Wetli, and J. Osterwalder, Rev. Sci. Instrum. **68**, 4549 (1997).

[16] M. Hengsberger, F. Baumberger, H. J. Neff, T. Greber, and J. Osterwalder, Phys. Rev. B **77**, 085425 (2008).

[17] C. Oshima and A. Nagashima, J. Phys. Condens. Matter **9**, 1 (1997).

[18] W. Auwärter, T. J. Kreutz, T. Greber, and J. Osterwalder, Surf. Sci. **429**, 229 (1999).

[19] D. Leuenberger, Master's thesis, University of Zurich, 2007.

[20] R. Fischer, S. Schuppler, N. Fischer, T. Fauster, and W. Steinmann, Phys. Rev. Lett. **70**, 654 (1993).

[21] U. Höfer, I. Shumay, C. Reuß, U. Thomann, W. Wallauer, and T. Fauster, Science **227**, 1480 (1997).

[22] G. B. Grad, P. Blaha, K. Schwarz, W. Auwärter, and T. Greber, Phys. Rev. B **68**, 085404 (2003).

[23] C. B. Harris, N. H. Ge, R. L. Lingle, J. D. McNeill, and C. M. Wong, Annu. Rev. Phys. Chem. **48**, 711 (1997).

[24] S. Schuppler, N. Fischer, W. Steinmann, R. Schneider, and E. Bertel, Phys. Rev. B **42**, 9403 (1990).

[25] A. Catellani, M. Posternak, A. Baldereschi, H. J. F. Jansen, and A. J. Freeman, Phys. Rev. B **32**, 6997 (1985).

[26] A. Catellani, M. Posternak, A. Baldereschi, and A. J. Freeman, Phys. Rev. B **36**, 6105 (1987).

[27] X. Blase, A. Rubio, S. G. Louie, and M. L. Cohen, Phys. Rev. B **51**, 6868 (1995).

[28] K. Watanabe and T. Taniguchi, Nat. Mater. **3**, 404 (2004).

[29] C. Cirelli, M. Hengsberger, A. Dolocan, H. Over, J. Osterwalder, and T. Greber, Europhys. Lett. **85**, 17010 (2009).

[30] S. Hellmann, K. Rossnagel, M. Marczynski-Bühlow, and L. Kipp, Phys. Rev. B **79**, 035402 (2009).

[31] J. Robertson, Phys. Rev. B **29**, 2131 (1984).

[32] W. Eberhardt and F. J. Himpsel, Phys. Rev. B **21**, 5572 (1980).

[33] M. Wolf, A. Hotzel, E. Knoesel, and D. Velic, Phys. Rev. B **59**, 5926 (1999).